

QUALITATIVE AND ANALYTICAL RESULTS OF THE BIFURCATION THRESHOLDS TO HALO ORBITS

SARA BUCCIARELLI, MARTA CECCARONI, ALESSANDRA CELLETTI,
AND GIUSEPPE PUCACCO

ABSTRACT. We study the dynamics in the neighborhood of the collinear Lagrangian points in the spatial, circular, restricted three–body problem. We consider the case in which one of the primaries is a radiating body and the other is oblate (although the latter is a minor effect). Beside having an intrinsic mathematical interest, this model is particularly suited for the description of a mission of a spacecraft (e.g., a solar sail) to an asteroid.

The aim of our study is to investigate the occurrence of bifurcations to halo orbits, which take place as the energy level is varied. The estimate of the bifurcation thresholds is performed by analytical and numerical methods: we find a remarkable agreement between the two approaches. As a side result, we also evaluate the influence of the different parameters, most notably the solar radiation pressure coefficient, on the dynamical behavior of the model.

To perform the analytical and numerical computations, we start by implementing a center manifold reduction. Next, we estimate the bifurcation values using qualitative techniques (e.g. Poincaré surfaces, frequency analysis, FLIs). Concerning the analytical approach, following [4] we implement a resonant normal form, we transform to suitable action-angle variables and we introduce a detuning parameter measuring the displacement from the synchronous resonance. The bifurcation thresholds are then determined as series expansions in the detuning. Three concrete examples are considered and we find in all cases a very good agreement between the analytical and numerical results.

CONTENTS

1. Introduction	2
2. The three–body problem with an oblate primary and SRP	5
2.1. The equations of motion	5
2.2. The equilibrium points	6
3. Linear stability of the collinear points and reduction of the quadratic part	7
3.1. Expansion of the Hamiltonian to fourth order	8
3.2. Reduction of the quadratic terms and linear stability	9
4. Center manifold reduction	11
4.1. Reduction to the center manifold	12

2010 *Mathematics Subject Classification.* 37N05, 70F15, 37L10.

Key words and phrases. Collinear Lagrangian points, Center manifolds, Halo orbits.

5. Analytical estimates of the bifurcation thresholds	13
6. Qualitative analysis of the bifurcation values	15
6.1. Poincaré section	16
6.2. Frequency analysis	16
6.3. Fast Lyapunov Indicator	16
6.4. Applications	17
7. Analytical versus numerical results	23
Acknowledgments	24
Appendix A. Derivation of the mean motion around an oblate primary	24
Appendix B. Reduction of the quadratic part	25
Appendix C. Center manifold reduction	26
References	28

1. INTRODUCTION

We consider the motion of a small body with negligible mass in the gravitational field of two primaries which move on circular trajectories around their common barycenter. We refer to this model as the *spatial, circular, restricted three–body problem* (hereafter SCR3BP). As it is well known (see, e.g., [20]), the SCR3BP admits five equilibrium positions in the synodic reference frame, which rotate with the angular velocity of the primaries. Two of such positions make an equilateral triangle with the primaries, while the other three equilibria are collinear with the primaries.

While the triangular positions are shown to be stable for a wide range of the mass ratio of the primaries, the collinear points are unstable. Nevertheless, the collinear equilibria turn out to be very useful in low–energy space missions and particular attention has been given to the so–called *halo orbits*, which are periodic trajectories around the collinear points, generated when increasing the energy level as bifurcations from the so–called *planar Lyapunov family* of periodic orbits.

We will consider a model in which one of the primaries (e.g. the Sun) is radiating; we will see that in some cases the effect of the solar radiation pressure (hereafter SRP) on a *solar sail*, namely an object with a high value of the area-to-mass ratio, is to lower the bifurcation threshold, enabling bifurcations before unfeasible. For sake of generality, we also consider the case in which the other primary is oblate, although this effect is definitely negligible in many concrete applications ([19]). We will consider the following three case

studies. The first one describes the interaction between the Earth–Moon barycenter and the Sun; we will refer to this case as the *Sun–barycenter* system. The second sample is provided by the Earth–Moon system. The last case describes the interaction between the Sun and one of the largest asteroids, Vesta, for which the effect of SRP is very important.

Our model depends on three main parameters, which are the mass ratio μ of the primaries, the performance β of the sail providing the ratio between the acceleration of the radiation pressure to the gravitational acceleration of the main primary (equivalently, one can use the parameter $q = 1 - \beta$) and the oblateness denoted by A , defined as $A = J_2 r_e^2$, see [14], where J_2 is the so-called dynamical oblateness coefficient and r_e is the equatorial radius of the planet. We remark that the orientation of the sail is set to be perpendicular with respect to the direction joining it with the main primary, so that the system still preserves the Hamiltonian character and no dissipation is allowed. All results could be easily generalised to the case in which the orientation of the sail is kept constant (i.e., non necessarily perpendicular) with respect to the direction joining it with the main primary as the system would still keep its Hamiltonian nature.

The aim of this paper is to make concrete analytical estimates of the bifurcations to halo orbits based on an extension of the theory developed in [4] and to compare the mathematical results with a qualitative investigation of the dynamics. As a side result, we shall evaluate the role of the parameters of the model, in particular the solar radiation pressure coefficient and the oblateness.

The collinear points with SRP and oblateness are shown to be of *saddle × center × center* type for typical parameter values (compare with Sections 2 and 3). According to widespread techniques, the dynamics can be conveniently described after having applied a reduction to the center manifold, which allows us to remove the hyperbolic components. The procedure consists in applying suitable changes of variables to reduce the Hamiltonian function to a simpler form and then to compute a Lie series transformation to get rid of the hyperbolic direction (see, e.g., [11], [10]). This procedure is performed in Sections 3 and 4, taking care of the modifications required by the consideration of the SRP and of the oblateness. Once the center manifold Hamiltonian has been obtained, we proceed to implement some numerical methods to investigate the dynamics as the energy level is varied, precisely we compute some Poincaré surfaces of section, we perform a frequency analysis and we determine the Fast Lyapunov Indicators ([12, 13, 6]). The independent and complementary application of the three methods has several advantages, as it helps to unveil many details of the complicated structures arising around the bifurcation values.

As for the analytical estimates (see [4]), after the center manifold reduction we need also to construct a fourth order normal form around the synchronous resonance. After introducing a coordinate change to action–angle variables for the quadratic part of the Hamiltonian, we recognize the existence of a first integral of motion. Finally, we introduce a quantity called *detuning*, which measures the (small) discrepancy of the frequencies around the synchronous resonance. The bifurcation threshold will then be computed at the first order in the powers series expansion in the detuning (see Section 5). We stress that, although we consider just the first non-trivial order of the expansion in the detuning, the analytical estimates are already in remarkable agreement with the numerical expectation (see Table 4). Clearly, more refined analytical results can be obtained computing higher order normal forms, at the expense of a bigger computational effort and provided the results are performed within the *optimal* order of normalization.

To conclude, let us mention that our comparison is made on the three case studies mentioned before (Sun–barycenter, Earth–Moon, Sun–Vesta); however, we provide full details only for the Sun–Vesta case, since the other two samples have been already investigated in the literature with an extensive use of the Poincaré maps (see, e.g., [8, 11]). The reason to focus on the case of Vesta is the following: due to the fact that Vesta has a relatively small mass, the interplay of the parameters gives rise to an interesting and non-trivial dynamical behavior (see Section 6.4). Indeed, in the Sun–Vesta case we shall see that the SRP plays an important effect, enabling more bifurcations at relatively low energy levels.

In fact, in the purely gravitational model only the first bifurcation (the *standard halo*) occurs in general ([8]), when the frequency of the planar Lyapunov orbit is the same as the frequency of its vertical perturbation. A second bifurcation, in which the planar Lyapunov trajectory regains stability and a second unstable family appears, is a rather extreme phenomenon at high energy values. In the presence of SRP this second bifurcation occurs instead at a much lower value of the energy. Moreover, also a third bifurcation may occur in which the *vertical* Lyapunov loses stability and the second family disappears. We will show how it is possible to predict the influence of SRP on the thresholds with a first-order perturbation approach.

This paper is organized as follows. In Section 2 we introduce the equations of motion and we determine the equilibrium points, whose linear stability as the parameters are varied is discussed in Section 3, where we prepare the Hamiltonian for the center manifold

reduction of Section 4. The analytical method to determine the bifurcation thresholds is presented in Section 5, while in Section 6 we implement the qualitative techniques, namely Poincaré maps, frequency analysis and Fast Lyapunov Indicators. The comparison between the analytical and numerical approaches, as well as some conclusions, are given in Section 7.

2. THE THREE-BODY PROBLEM WITH AN OBLATE PRIMARY AND SRP

In this section we start by introducing the equations of motion describing the SCR3BP with a radiating larger primary and an oblate smaller primary (see Section 2.1). Then, we proceed to compute the location of the collinear equilibrium points as a function of the parameters μ, β, A (see Section 2.2).

2.1. The equations of motion. Let us denote by μ and $1-\mu$ the masses of the primaries with $\mu \in (0, 1/2]$ and let us assume the units of measure, so that the gravitational constant is unity and the period of the primaries is equal to 2π . We consider a synodic reference system (O, X, Y, Z) , rotating with the angular velocity of the primaries, with the origin located at the barycenter of the primaries and the abscissa along the primaries' axis. The position of the smaller primary is at $(-1 + \mu, 0, 0)$, while the larger primary is located at $(\mu, 0, 0)$. Let (X, Y, Z) be the coordinates of the third body in this reference frame. Let (P_X, P_Y, P_Z) be the conjugated kinetic momenta defined as $P_X = \dot{X} - nY$, $P_Y = \dot{Y} + nX$, $P_Z = \dot{Z}$, where n denotes the mean motion, $n = 2\pi/T_{rev}$ and T_{rev} is the period of revolution.

The equations of motion are given by

$$\begin{aligned}\ddot{X} - 2n\dot{Y} &= \frac{\partial \Omega}{\partial X} \\ \ddot{Y} + 2n\dot{X} &= \frac{\partial \Omega}{\partial Y} \\ \ddot{Z} &= \frac{\partial \Omega}{\partial Z},\end{aligned}\tag{2.1}$$

where

$$\Omega = \Omega(X, Y, Z) \equiv \frac{n^2}{2}(X^2 + Y^2) + \frac{q(1-\mu)}{r_1} + \frac{\mu}{r_2} \left[1 + \frac{A}{2r_2^2} \left(1 - \frac{3Z^2}{r_2^2} \right) \right]$$

with the mean motion given by $n = \sqrt{1 + \frac{3}{2}A}$ (compare with Appendix A), while the distances r_1, r_2 from the primaries are given by $r_1 = \sqrt{(X - \mu)^2 + Y^2 + Z^2}$ and $r_2 = \sqrt{(X - \mu + 1)^2 + Y^2 + Z^2}$ (see, e.g., [5, 15]). We have used $q = 1 - \beta$, where the

performance β of the sail is defined by

$$\beta \equiv \frac{L_{\odot}Q}{4\pi c GM_{\odot}B} ,$$

where $L_{\odot} = 3.839 \times 10^{26}$ Watt is the Sun luminosity, Q is one plus the reflectivity, c is the speed of light, G is the gravitational constant, M_{\odot} the Solar mass and B the mass/area ratio of the spacecraft.

Notice that equations (2.1) are associated to the following Hamiltonian function:

$$\begin{aligned} H(X, Y, Z, P_X, P_Y, P_Z) = & \frac{1}{2}(P_X^2 + P_Y^2 + P_Z^2) + nYP_X - nXP_Y - \frac{q(1-\mu)}{r_1} \\ & - \frac{\mu}{r_2} \left[1 + \frac{A}{2r_2^2} \left(1 - \frac{3Z^2}{r_2^2} \right) \right] . \end{aligned} \quad (2.2)$$

2.2. The equilibrium points. It is well known (see, e.g., [20]) that the circular, restricted three-body problem admits the Lagrangian equilibrium points, precisely the triangular solutions, denoted as L_4 and L_5 , and the collinear solutions, denoted as L_1 , L_2 , L_3 , the latter being located on the axis joining the primaries. Due to the oblateness and to the radiation pressure effects, out-of-plane equilibria can be found in the spatial case (see [5]), but we will not consider such solutions in the present work.

To locate the equilibrium positions we impose that the derivatives of Ω in these points are zero, say $\frac{\partial\Omega}{\partial X} = \frac{\partial\Omega}{\partial Y} = \frac{\partial\Omega}{\partial Z} = 0$. In particular, we obtain:

$$\begin{aligned} \frac{\partial\Omega}{\partial Y} = & n^2Y - \frac{qY(1-\mu)}{(Y^2 + Z^2 + (X-\mu)^2)^{\frac{3}{2}}} + \frac{15AYZ^2\mu}{2(Y^2 + Z^2 + (1+X-\mu)^2)^{\frac{7}{2}}} \\ & - \frac{3AY\mu}{2(Y^2 + Z^2 + (1+X-\mu)^2)^{\frac{5}{2}}} - \frac{Y\mu}{(Y^2 + Z^2 + (1+X-\mu)^2)^{\frac{3}{2}}} , \end{aligned}$$

so that we have $\frac{\partial\Omega}{\partial Y} = 0$ whenever $Y = 0$. In a similar way we obtain:

$$\begin{aligned} \frac{\partial\Omega}{\partial Z} = & -\frac{qZ(1-\mu)}{(Y^2 + Z^2 + (X-\mu)^2)^{\frac{3}{2}}} + \frac{15AZ^3\mu}{2(Y^2 + Z^2 + (1+X-\mu)^2)^{\frac{7}{2}}} \\ & - \frac{9AZ\mu}{2(Y^2 + Z^2 + (1+X-\mu)^2)^{\frac{5}{2}}} - \frac{Z\mu}{(Y^2 + Z^2 + (1+X-\mu)^2)^{\frac{3}{2}}} \end{aligned}$$

and we have $\frac{\partial\Omega}{\partial Z} = 0$ whenever $Z = 0$. As for the derivative with respect to the first component, we have:

$$\begin{aligned} \frac{\partial\Omega}{\partial X} = & n^2X - \frac{q(1-\mu)(X-\mu)}{(Y^2 + Z^2 + (X-\mu)^2)^{\frac{3}{2}}} + \frac{15AZ^2\mu(1+X-\mu)}{2(Y^2 + Z^2 + (1+X-\mu)^2)^{\frac{7}{2}}} \\ & - \frac{3A(1+X-\mu)\mu}{2(Y^2 + Z^2 + (1+X-\mu)^2)^{\frac{5}{2}}} - \frac{(1+X-\mu)\mu}{(Y^2 + Z^2 + (1+X-\mu)^2)^{\frac{3}{2}}} . \end{aligned} \quad (2.3)$$

Inserting $Y = Z = 0$ in (2.3) we get the equation

$$n^2 X - \frac{q(1-\mu)(X-\mu)}{|X-\mu|^3} - \frac{3A\mu(1+X-\mu)}{2|1+X-\mu|^5} - \frac{\mu(1+X-\mu)}{|1+X-\mu|^3} = 0. \quad (2.4)$$

Let us denote by γ_j the distance between L_j and the closer primary. Since the collinear points L_1, L_2, L_3 lie in the intervals $(-1+\mu, \mu)$, $(-\infty, -1+\mu)$, $(\mu, +\infty)$, setting $X = \gamma_1 + \mu - 1$ for L_1 , $X = -\gamma_2 + \mu - 1$ for L_2 , $X = \gamma_3 + \mu$ for L_3 , the quantity γ_j is found as the unique positive solution of the following generalized Euler's equations:

$$\begin{aligned} \pm & 2n^2\gamma_j^7 + (2n^2\mu - 6n^2)\gamma_j^6 \pm (6n^2 - 4n^2\mu)\gamma_j^5 + (2n^2\mu - 2q\mu - 2n^2 + 2q \mp 2\mu)\gamma_j^4 \\ & + 4\mu\gamma_j^3 \mp (2\mu + 3A\mu)\gamma_j^2 + 6A\mu\gamma_j \mp 3A\mu = 0 \end{aligned}$$

for $j = 1, 2$, where the upper sign holds for L_1 , while the lower sign holds for L_2 ; as for L_3 , we have that γ_3 is the solution of the following Euler's equation

$$\begin{aligned} & 2n^2\gamma_3^7 + (8n^2 + 2n^2\mu)\gamma_3^6 + (12n^2 + 8n^2\mu)\gamma_3^5 + (8n^2 + 2q\mu + 12n^2\mu - 2q - 2\mu)\gamma_3^4 \\ & + (2n^2 - 8q - 4\mu + 8n^2\mu + 8q\mu)\gamma_3^3 + (2n^2\mu - 3A\mu + 12q\mu - 12q - 2\mu)\gamma_3^2 \\ & + (8q\mu - 8q)\gamma_3 + 2q\mu - 2q = 0. \end{aligned}$$

Making use of equation (2.4), we show below the dependence of the location of the collinear points as the parameters (μ, A, β) are varied, where we assume that the parameters belong to the following intervals^{1,2}:

$$0 < \mu \leq 0.5, \quad 0 \leq A \leq 10^{-4}, \quad 0 \leq \beta \leq 0.5. \quad (2.5)$$

Here and in the following sections we consider three paradigmatic cases, which correspond to a spacecraft or a solar sail orbiting in the Earth–Moon system, in the Sun–barycenter system and in the Sun–Vesta system; these three cases encompass missions to satellites, planets or asteroids and are characterized by different values of the parameters as well as by different distances of the collinear points, as reported in Table 2.

3. LINEAR STABILITY OF THE COLLINEAR POINTS AND REDUCTION OF THE QUADRATIC PART

To study the stability of the collinear equilibrium points and their dependency on the parameters, we compute the linearization of the equations of motion, which requires

¹The upper bound on A , say $A \leq 10^{-4}$, is definitely large for solar system bodies, but it might apply to extrasolar planetary systems.

²A realistic upper bound on the sail performance should be $\beta \leq 0.1$; however, we consider β up to 0.5 as it is often done in the literature, see e.g., [9].

to expand the Hamiltonian in series up to the second order. Indeed, we will expand it directly up to the fourth order as this will be used for the reduction to the center manifold in Section 4. Although the computation of the linear stability is rather elementary, it is mandatory before performing the center manifold reduction as in Section 4.

3.1. Expansion of the Hamiltonian to fourth order. We shift and scale the equilibrium points by making the following transformation ([11]):

$$X = \mp \gamma_j x + \mu + \alpha , \quad Y = \mp \gamma_j y , \quad Z = \gamma_j z , \quad (3.1)$$

where γ_j denotes again the distance of L_j from the closer primary; the upper sign corresponds to $L_{1,2}$ and the lower sign to L_3 , while $\alpha \equiv -1 + \gamma_1$ for L_1 , $\alpha \equiv -1 - \gamma_2$ for L_2 and $\alpha \equiv \gamma_3$ for L_3 . These conventions will hold hereafter. It must be remarked that, in all cases, the transformation (3.1) is symplectic of parameter γ_j^2 , so that the resulting Hamiltonian must be divided by such factor. Inserting (3.1) in (2.3), we have:

$$\frac{\partial \Omega}{\partial X} = n^2 X + \frac{\partial}{\partial X} \left[\frac{q(1-\mu)}{r_1} + \frac{\mu}{r_2} + \frac{A\mu}{2r_2^3} - \frac{3\gamma_1^2 z^2 A\mu}{2r_2^5} \right] ;$$

therefore, we obtain the equation of motion:

$$\mp \ddot{x} \pm 2n\dot{y} \pm n^2 x = \frac{n^2(\mu + \alpha)}{\gamma_j} \mp \frac{1}{\gamma_j^2} \frac{\partial}{\partial x} \left[\frac{q(1-\mu)}{r_1} + \frac{\mu}{r_2} + \frac{A\mu}{2r_2^3} - \frac{3\gamma_j^2 z^2 A\mu}{2r_2^5} \right] ,$$

where $j = 1, 2, 3$. We remark that the inverse of the distances are transformed as

$$\frac{1}{r_1} = \frac{1}{\gamma_j \sqrt{(x \mp \frac{\alpha}{\gamma_j})^2 + y^2 + z^2}} , \quad \frac{1}{r_2} = \frac{1}{\gamma_j \sqrt{(-x \pm \frac{\alpha+1}{\gamma_j})^2 + y^2 + z^2}} .$$

In a similar way, for the other two components we obtain:

$$\begin{aligned} \mp \gamma_j \ddot{y} \mp 2n\gamma_j \dot{x} &= \mp n^2(\gamma_j y) \mp \frac{1}{\gamma_j} \frac{\partial}{\partial y} \left[\frac{q(1-\mu)}{r_1} + \frac{\mu}{r_2} + \frac{A\mu}{2r_2^3} - \frac{3\gamma_1^2 z^2 A\mu}{2r_2^5} \right] \\ \gamma_j \ddot{z} &= \frac{1}{\gamma_j} \frac{\partial}{\partial z} \left[\frac{q(1-\mu)}{r_1} + \frac{\mu}{r_2} + \frac{A\mu}{2r_2^3} - \frac{3\gamma_1^2 z^2 A\mu}{2r_2^5} \right] . \end{aligned}$$

Expanding in Taylor series $1/r_1$, $1/r_2$ and their powers, we compute the linearized equations as

$$\begin{aligned} \ddot{x} - 2n\dot{y} - (n^2 - 2a)x &= 0 \\ \ddot{y} + 2n\dot{x} + (-n^2 + b)y &= 0 \\ \ddot{z} + cz &= 0 , \end{aligned}$$

where the quantities a , b , c take different values according to the considered equilibrium point. Since in the following sections we shall analyze only L_1 and L_2 , we provide the

explicit values for such positions. Precisely, one has:

$$\begin{aligned} a &= \frac{q(1-\mu)}{\alpha^3} \mp \frac{\mu}{(1+\alpha)^3} \mp \frac{3A\mu}{(1+\alpha)^5} \\ b &= -\frac{q(1-\mu)}{\alpha^3} \pm \frac{\mu}{(1+\alpha)^3} \pm \frac{3A\mu}{2(1+\alpha)^5} \\ c &= -\frac{q(1-\mu)}{\alpha^3} \pm \frac{\mu}{(1+\alpha)^3} \pm \frac{9A\mu}{2(1+\alpha)^5}, \end{aligned}$$

where the upper sign holds for L_1 and the lower sign for L_2 .

Setting for shortness $\Delta \equiv \frac{3A\mu}{2(1+\alpha)^5}$, we can write a and c in terms of b as

$$a = -(b + \Delta), \quad c = b + 2\Delta. \quad (3.2)$$

It results that $\Delta > 0$ and $b > 0$ for all $A > 0$, $\mu > 0$, $\beta > 0$.

Finally, the complete equations of motion in the new variables can be written as

$$\begin{aligned} \ddot{x} - 2n\dot{y} - (n^2 - 2a)x &= \frac{1}{\gamma_j^2} \frac{\partial}{\partial x} \sum_{n \geq 3} H_n \\ \ddot{y} + 2n\dot{x} + (-n^2 + b)y &= \frac{1}{\gamma_j^2} \frac{\partial}{\partial y} \sum_{n \geq 3} H_n \\ \ddot{z} + cz &= \frac{1}{\gamma_j^2} \frac{\partial}{\partial z} \sum_{n \geq 3} H_n, \end{aligned} \quad (3.3)$$

where H_n are suitable polynomials of degree n . Defining the momenta as $p_x = \dot{x} - ny$, $p_y = \dot{y} + nx$, $p_z = \dot{z}$ and using (3.3), the Hamiltonian function (2.2) becomes

$$H(x, y, z, p_x, p_y, p_z) = \frac{1}{2}(p_x^2 + p_y^2 + p_z^2) + nyp_x - nxp_y + ax^2 + \frac{1}{2}by^2 + \frac{1}{2}cz^2 - \frac{1}{\gamma_j^2} \sum_{n \geq 3} H_n. \quad (3.4)$$

3.2. Reduction of the quadratic terms and linear stability. The quadratic part of the Hamiltonian (3.4) is given by

$$H_2(x, y, z, p_x, p_y, p_z) = \frac{1}{2}(p_x^2 + p_y^2) + nyp_x - nxp_y + \frac{1}{2}p_z^2 + ax^2 + \frac{1}{2}by^2 + \frac{1}{2}cz^2.$$

By (3.2) it results that $c > 0$ for each of the equilibrium points. This implies that the vertical direction is described by a harmonic oscillator with frequency $\omega_2 = \sqrt{c}$, namely:

$$\dot{p}_z = -\frac{\partial H}{\partial z} = -cz, \quad \dot{z} = \frac{\partial H}{\partial p_z} = p_z.$$

As for the planar directions, following [11] the quadratic part of the Hamiltonian, that we keep denoting as H_2 , is given by

$$H_2(x, y, p_x, p_y) = \frac{1}{2}(p_x^2 + p_y^2) + nyp_x - nxp_y + ax^2 + \frac{1}{2}by^2.$$

Denoting by J the symplectic matrix, the equations of motion are given by

$$\begin{pmatrix} \dot{x} \\ \dot{y} \\ \dot{p}_x \\ \dot{p}_y \end{pmatrix} = J \text{Hess}(H_2) \begin{pmatrix} x \\ y \\ p_x \\ p_y \end{pmatrix} = \begin{pmatrix} 0 & n & 1 & 0 \\ -n & 0 & 0 & 1 \\ -2a & 0 & 0 & n \\ 0 & -b & -n & 0 \end{pmatrix} \begin{pmatrix} x \\ y \\ p_x \\ p_y \end{pmatrix}.$$

Let us define the matrix M as

$$M \equiv J \text{Hess}(H_2); \quad (3.5)$$

the associated characteristic polynomial is given by

$$p(\lambda) = \lambda^4 + (2n^2 + 2a + b)\lambda^2 + (n^4 - 2an^2 - bn^2 + 2ab). \quad (3.6)$$

Setting $\eta = \lambda^2$, the roots of the polynomial (3.6) are given by

$$\begin{aligned} \eta_1 &= \frac{-2n^2 - 2a - b - \sqrt{16an^2 + 4a^2 + 8bn^2 - 4ab + b^2}}{2} \\ \eta_2 &= \frac{-2n^2 - 2a - b + \sqrt{16an^2 + 4a^2 + 8bn^2 - 4ab + b^2}}{2}. \end{aligned}$$

In order to study the stability of the collinear equilibrium points we have to establish the domains in which $\lambda_{1,3} = \pm\sqrt{\eta_1}$ and $\lambda_{2,4} = \pm\sqrt{\eta_2}$ are real, complex or imaginary. In particular, a given equilibrium point L_j will be linearly stable, if η_1 and η_2 are purely imaginary, while it is unstable elsewhere. We are interested to the case in which the collinear points are of the type *saddle* \times *center* \times *center*, which occurs whenever $\eta_1 < 0$ and $\eta_2 > 0$. This is equivalent to require that the following inequalities are satisfied:

$$\begin{cases} 16an^2 + 4a^2 + 8bn^2 - 4ab + b^2 \geq 0 \\ -2n^2 - 2a - b + \sqrt{16an^2 + 4a^2 + 8bn^2 - 4ab + b^2} > 0 \\ -2n^2 - 2a - b - \sqrt{16an^2 + 4a^2 + 8bn^2 - 4ab + b^2} < 0. \end{cases}$$

Using (3.2), the inequalities (3.7) become:

$$\begin{cases} 9b^2 + 4\Delta(-4n^2 + \Delta) + b(-8n^2 + 12\Delta) \geq 0 \\ b - 2n^2 + 2\Delta + \sqrt{9b^2 + 4\Delta(-4n^2 + \Delta) + b(-8n^2 + 12\Delta)} > 0 \\ b - 2n^2 + 2\Delta - \sqrt{9b^2 + 4\Delta(-4n^2 + \Delta) + b(-8n^2 + 12\Delta)} < 0. \end{cases} \quad (3.7)$$

The first condition in (3.7) is satisfied whenever

$$b > \frac{2}{9}(2n^2 - 3\Delta + 2\sqrt{n^4 + 6n^2\Delta}). \quad (3.8)$$

Given that the function at the right hand side of (3.8) reaches its maximum n^2 for $\Delta = \frac{n^2}{2}$, the inequality (3.8) is verified if $b > n^2 = \sqrt{1 + \frac{3}{2}A}$. The second and third conditions in (3.7) can be reduced to verify just that

$$8b^2 + b(8\Delta - 4n^2) - 8n^2\Delta - 4n^4 > 0,$$

which is satisfied again if $b > n^2$, which holds for all values of the oblateness, the solar radiation pressure and the mass parameter in the intervals defined in (2.5). This concludes the discussion of the stability character of the collinear points, including the solar radiation pressure and the oblateness of one of the primaries.

4. CENTER MANIFOLD REDUCTION

Due to the *saddle* \times *center* \times *center* character of the collinear equilibrium points (see Section 3), we proceed to perform the reduction to the center manifold. The adopted procedure is a straightforward extension of that used in [11], provided that we include the necessary modifications to consider the effects of the oblateness and the solar radiation pressure. For completeness, we report here the main steps to treat the Hamiltonian (2.2) (see Appendix C for more details). We stress that after removing the hyperbolic direction, we will be able to perform a qualitative analysis based on Poincaré sections, frequency analysis and Fast Lyapunov Indicators as it is done in Section 6.

Taking into account that $\eta_1 < 0$ and $\eta_2 > 0$, let $\omega_1 = \sqrt{-\eta_1}$ and $\lambda_1 = \sqrt{\eta_2}$; we look for a change of variables, so that we reach a simpler form of the Hamiltonian. As described in detail in Appendix B, this is obtained by computing the eigenvalues and eigenvectors of M in (3.5), which provide a transformation allowing to get a Hamiltonian with the following quadratic part (with a slight abuse we keep the same notation for all variables):

$$H_2(x, y, z, p_x, p_y, p_z) = \lambda_1 x p_x + \frac{\omega_1}{2} (p_y^2 + y^2) + \frac{\omega_2}{2} (p_z^2 + z^2) , \quad (4.1)$$

where

$$\begin{aligned} \lambda_1 &= \sqrt{\frac{-2n^2 - 2a - b + \sqrt{16an^2 + 4a^2 + 8bn^2 - 4ab + b^2}}{2}} \\ \omega_1 &= \sqrt{\frac{-2n^2 - 2a - b - \sqrt{16an^2 + 4a^2 + 8bn^2 - 4ab + b^2}}{2}} \\ \omega_2 &= \sqrt{c} . \end{aligned}$$

In analogy to [11], we introduce the following complex transformation

$$\begin{aligned} x &= q_1, & y &= \frac{q_2 + ip_2}{\sqrt{2}}, & z &= \frac{q_3 + ip_3}{\sqrt{2}} \\ p_x &= p_1, & p_y &= \frac{iq_2 + p_2}{\sqrt{2}}, & p_z &= \frac{iq_3 + p_3}{\sqrt{2}} , \end{aligned}$$

which provides a complex expression for the Hamiltonian; we report here the quadratic part of the Hamiltonian, which takes the form:

$$H_2(q_1, q_2, q_3, p_1, p_2, p_3) = \lambda_1 q_1 p_1 + i\omega_1 q_2 p_2 + i\omega_2 q_3 p_3 . \quad (4.2)$$

Beside the quadratic part (4.2), we need to compute the nonlinear terms. Straightforward but tedious computations, performed by means of the **Mathematica**[©] algebraic manipulator, allow us to find the expressions of H_3 and H_4 in complex variables. Afterwards we shall implement a Lie series transformation to obtain the reduction to the center manifold as described in the following section.

4.1. Reduction to the center manifold. The reduction to the center manifold is obtained by making suitable changes of variables by using Lie series (see Appendix C). Indeed, we conjugate the SCR3BP to a Hamiltonian of the form

$$H(q, p) = \lambda_1 q_1 p_1 + i\omega_2 q_2 p_2 + i\omega_3 q_3 p_3 + \sum_{n \geq 3} H_n(q, p) ,$$

for suitable coordinates (q_1, q_2, q_3) and momenta (p_1, p_2, p_3) , where the quadratic part has been obtained in (4.2) and H_n denotes a homogeneous polynomial of degree n . In the linear approximation the center manifold is obtained by imposing $q_1 = p_1 = 0$, since the hyperbolicity pertains to such variables. Then, we will require that $\dot{q}_1(0) = \dot{p}_1(0) = 0$ for $q_1(0) = p_1(0) = 0$, so that we obtain $q_1(t) = p_1(t) = 0$ for any time, due to the autonomous character of the problem. Taking into account Hamilton's equations

$$\dot{q}_i = H_{p_i} , \quad \dot{p}_i = -H_{q_i} ,$$

this requirement is satisfied whenever in the series expansion of the Hamiltonian all monomials of the type $h_{ij}q^i p^j$ with $i_1 \neq j_1$ are such that $h_{ij} = 0$, being $i = (i_1, i_2, i_3)$ and $j = (j_1, j_2, j_3)$. In this way we obtain a Hamiltonian of the form $H(q, p) = H_N(q, p) + R_N(q, p)$, where $H_N(q, p)$ is a polynomial of degree N in (q, p) without terms depending on the product $q_1 p_1$, while $R_N(q, p)$ is a reminder of order $N+1$. We refer to Appendix C for the description of a procedure based on Lie series to determine explicitly the required canonical transformation. Let us denote by (y, z, p_y, p_z) the normalized variables; the final expression of the Hamiltonian reduced to the center manifold has the following form:

$$\tilde{H}(y, z, p_y, p_z) = \frac{\omega_1}{2}(p_y^2 + y^2) + \frac{\omega_2}{2}(p_z^2 + z^2) + \tilde{H}_3(y, z, p_y, p_z) + \tilde{H}_4(y, z, p_y, p_z) , \quad (4.3)$$

where \tilde{H}_3 , \tilde{H}_4 denote homogeneous polynomials of degree, respectively, 3 and 4. The frequencies ω_1 , ω_2 , as well as those of the higher order terms, depend on the choice of the parameters and will be specified in each concrete case.

5. ANALYTICAL ESTIMATES OF THE BIFURCATION THRESHOLDS

Analytical results providing an estimate for the value of the thresholds at which the bifurcation of halo orbits takes place have been presented in [4]. The result is briefly summarized as follows. After the reduction to the center manifold, a normal form is computed around the synchronous resonance. The resulting normal form admits a first integral, related to the action variables of the harmonic oscillator (i.e., the quadratic part in (4.3)). A detuning measuring the displacement around the synchronous resonance is introduced; assuming that the detuning is small, one can compute the bifurcation threshold at different orders in the powers series expansion in the detuning. In [4] the computation at first and second order has been performed. Here, we extend the method of [4] by computing the thresholds for the model including oblateness and solar radiation pressure. As we will see in Section 6, the case in which the parameter β is different from zero allows one to find several bifurcations at relatively low energy levels. We anticipate that the analytical estimates computed in this section will agree with the numerical values of Section 6 (see Table 4).

Let us write (4.3) in complex form, implementing the following change of coordinates:

$$\begin{aligned} Q_2 &= \frac{\sqrt{2}}{2i}(p_2 + iq_2) , & Q_3 &= \frac{\sqrt{2}}{2i}(p_3 + iq_3) , \\ P_2 &= \frac{\sqrt{2}}{2}(p_2 - iq_2) , & P_3 &= \frac{\sqrt{2}}{2}(p_3 - iq_3) . \end{aligned}$$

Next, we introduce action-angle variables $(I_2, I_3, \theta_2, \theta_3)$ for the quadratic part of the Hamiltonian by means of the change of coordinates:

$$\begin{aligned} Q_2 &= -i\sqrt{I_2} e^{i\theta_2} , & Q_3 &= -i\sqrt{I_3} e^{i\theta_3} , \\ P_2 &= \sqrt{I_2} e^{-i\theta_2} , & P_3 &= \sqrt{I_3} e^{-i\theta_3} , \end{aligned}$$

so that we obtain a Hamiltonian of the form

$$H(\theta_2, \theta_3, I_2, I_3) = \omega_2 I_2 + \omega_3 I_3 + \tilde{H}_3(\theta_2, \theta_3, I_2, I_3) + \tilde{H}_4(\theta_2, \theta_3, I_2, I_3) .$$

To investigate the appearance of the resonant periodic orbits we compute a normal form in the neighborhood of the synchronous resonance $\omega_2 = \omega_3$. The explicit computation

TABLE 1. Coefficients of the normal form (5.1) around L_1 for the Earth–Moon, Sun–barycenter, Sun–Vesta systems with and without solar radiation pressure.

	a_{20}	a_{02}	a_{11}	b_{11}
Earth–Moon	0.162109	0.144891	0.0726274	0.116537
Sun–barycenter $\beta = 0$	0.0989667	0.08098	−0.0256235	0.102138
Sun–barycenter $\beta = 10^{-2}$	0.136123	0.108011	0.0189407	0.11106
Sun–Vesta $\beta = 0$	0.0957347	0.0777063	−0.0304854	0.101319
Sun–Vesta $\beta = 10^{-2}$	0.0157472	0.00203253	$4.11966 \cdot 10^{-7}$	0.00533371

shows that the first non–trivial order is given by \tilde{H}_4 , since the third degree term \tilde{H}_3 does not contain resonant terms. We are thus led to a resonant normal form given by

$$H_{NF}(\theta_2, \theta_3, I_2, I_3) = \omega_2 I_2 + \omega_3 I_3 + \left[a_{20} I_2^2 + a_{02} I_3^2 + I_2 I_3 (a_{11} + 2b_{11} \cos(2\theta_2 - 2\theta_3)) \right], \quad (5.1)$$

where the coefficients a_{20} , a_{02} , a_{11} , b_{11} are evaluated explicitly in Table 1.

The dynamics is determined by the *normal modes* $I_k = \text{const.}$, $k = 2, 3$ and by the periodic orbits in general position, related to the resonance. The normal modes always exist and at low energies are both stable: $I_2 = \text{const.}$, $I_3 = 0$ gives rise to the *planar Lyapunov orbit*; $I_2 = 0$, $I_3 = \text{const.}$ gives rise to the *vertical Lyapunov orbit*. When stable, these orbits are surrounded by families of *Lissajous tori*. The resonant families may appear as bifurcation from the normal mode at some given energy threshold and are determined by the condition that the frequency of the normal mode is equal to that of its normal perturbation. The normal modes can be again stable through a second bifurcation; a concrete example of a second bifurcation for the Earth–Moon case is given in [8] (we refer to [4, 16, 17, 18] for further details). To investigate the possible sequences of bifurcations we proceed as follows.

From Hamilton’s equations associated to (5.1), it is readily seen that $\dot{I}_2 + \dot{I}_3 = 0$. This remark leads to introduce the following change of variables ([4]):

$$\begin{aligned} \mathcal{E} &= I_2 + I_3, & \mathcal{R} &= I_2, \\ \nu &= \theta_3, & \psi &= \theta_2 - \theta_3. \end{aligned} \quad (5.2)$$

Moreover, following [4] let us introduce the *detuning* δ as

$$\delta = \omega_2 - \omega_3,$$

which measures the displacement from the synchronous resonance. Using (5.2) the Hamiltonian (5.1) becomes

$$H_{\text{new}}(\mathcal{E}, \mathcal{R}, \nu, \psi) = \mathcal{E} + \tilde{\delta}\mathcal{R} + a\mathcal{R}^2 + b\mathcal{E}^2 + c\mathcal{E}\mathcal{R} + d(\mathcal{R}^2 - \mathcal{E}\mathcal{R}) \cos 2\psi ,$$

where $\tilde{\delta} = \delta/\omega_3$, $a = (a_{20} + a_{02} - a_{11})/\omega_3$, $b = a_{02}/\omega_3$, $c = (a_{11} - 2a_{02})/\omega_3$, $d = -2b_{11}/\omega_3$.

It has been shown in [4] that the equilibria associated to Hamilton's equations of H_{new} can be classified as *inclined* (or 'anti-halo') when $\psi = 0$ or $\psi = \pi$, and *loop* (or 'halo'), when $\psi = \pm\pi/2$. In view of the reflection symmetries, each case actually corresponds to a double family. They exist at the following level values of the integral of motion \mathcal{E} :

$$\mathcal{E}_{iy} = \frac{\delta\omega_2^2}{-a_{11} + 2(a_{20} - b_{11})} , \quad \mathcal{E}_{iz} = \frac{\delta\omega_2^2}{-2a_{02} + a_{11} + 2b_{11}} , \quad (5.3)$$

for the inclined families and

$$\mathcal{E}_{\ell y} = \frac{\delta\omega_2^2}{-a_{11} + 2(a_{20} + b_{11})} , \quad \mathcal{E}_{\ell z} = \frac{\delta\omega_2^2}{-2a_{02} - a_{11} + 2b_{11}} , \quad (5.4)$$

for the loop families. These values correspond to a first order computation in the detuning; refined (but more complicated) values at second order have been found analytically in [4].

The physical interpretation of the thresholds in (5.3), (5.4) is the following. The quantity $\mathcal{E}_{\ell y}$ determines the bifurcation of the halo families from the planar Lyapunov orbit, when this becomes unstable. At \mathcal{E}_{iy} the planar Lyapunov orbit turns back to being stable and one observes the bifurcation of the (unstable) anti-halo orbits. Finally, the two unstable families which have been formed collapse on the vertical at \mathcal{E}_{iz} . The disappearance of the halo at $\mathcal{E}_{\ell z}$ never occurs in all cases we have investigated.

This sequence of bifurcations will be clearly shown in the case of the asteroid Vesta under the effect of solar radiation pressure (see Section 6).

6. QUALITATIVE ANALYSIS OF THE BIFURCATION VALUES

On the basis of the center manifold reduction obtained in Section 4, we implement some numerical techniques which allow us to characterize the dynamics and, in particular, to distinguish between the different types of orbits, precisely planar Lyapunov and halo orbits, the latter ones obtained at specific levels of the energy at which the bifurcation takes place. As concrete models, we consider three paradigmatic cases, characterized by different values of the mass ratio: a relatively high value as in the Earth–Moon system, an intermediate mass ratio as for the Sun–barycenter system (between the barycenter of the Earth–Moon system and the Sun), and a low value as in the Sun–Vesta system.

6.1. Poincaré section. To get a qualitative description of the dynamics in the center manifold we start by computing a Poincaré section as follows. We set $z = 0$ and we fix an energy level $H = h_0$, from which we compute the initial value of p_z choosing the solution with $p_z > 0$. The Poincaré section is then shown in the plane (y, p_y) ; we will see that, as the energy increases and exceeds a specific energy value, halo orbits arise from bifurcations of planar Lyapunov periodic orbits.

6.2. Frequency analysis. This technique consists in studying the behavior of the *frequency map* ([12, 13]), which is obtained computing the variation of the absolute value of the ratio of the frequencies, say $\omega_r = |\omega_y/\omega_z|$, as a function of the initial values of the action variables, whereas the initial conditions of the angles can be set to zero (see, e.g., [3], see also [2]).

The frequency analysis has the advantage to be computationally fast and it allows us to obtain a complementary investigation of the occurrence of halo orbits. Precisely, we proceed as follows. Concerning the initial conditions, we fix as starting values $z = 0$ and $p_y = p_y^0$, we scan over initial values for y in a given interval and for an assigned energy level $H = h_0$, we compute the corresponding value of p_z . We find convenient to avoid using Cartesian variables, and we rather transform to action-angle variables for the quadratic part of (4.3). Thus, we introduce harmonic oscillator actions (J_y, J_z) defined through the expressions

$$\begin{aligned} p_y &= \sqrt{2J_y} \cos \theta_y, & y &= \sqrt{2J_y} \sin \theta_y, \\ p_z &= \sqrt{2J_z} \cos \theta_z, & z &= \sqrt{2J_z} \sin \theta_z, \end{aligned}$$

where (θ_y, θ_z) denote the conjugated angle variables. Next we perform a first order perturbation theory by averaging over the angle variables to obtain a normalized Hamiltonian, whose derivative provides an expression for the frequencies associated to the given initial conditions. Finally, we back-transform to the variables (J_y, J_z) to get a frequency vector (ω_y, ω_z) associated to the previous initial data. The frequency map is obtained by computing the variation of $\omega_r = |\omega_y/\omega_z|$ as the initial condition is varied.

6.3. Fast Lyapunov Indicator. In order to investigate the stability of the dynamics in the center manifold, we compute a quantity called the Fast Lyapunov Indicator (hereafter FLI), which is determined as the value of the largest Lyapunov characteristic exponent at a fixed time (see [6]). By comparing the values of the FLIs as the initial conditions or suitable parameters are varied, one obtains an indication of the dynamical character of the orbits (precisely Lyapunov or halo) as well as of their stability. The explicit

TABLE 2. Main parameters and location (in normalized units) of the collinear points for the Earth–Moon, Sun–barycenter, Sun–Vesta systems.

	Earth–Moon	Sun–barycenter	Sun–Vesta
μ	$1.2154 \cdot 10^{-2}$	$3.040423 \cdot 10^{-6}$	$1.3574 \cdot 10^{-10}$
J_2	$2.034 \cdot 10^{-4}$	$1081 \cdot 10^{-6}$	0.0812232
A	$4.15559 \cdot 10^{-9}$	$1.96782 \cdot 10^{-12}$	$4.54776 \cdot 10^{-14}$
β	0	10^{-2}	10^{-2}
L_1	-0.836898	-0.988731	-0.996651
L_2	-1.1557	-1.00908	-1.000115
L_3	1.00506	0.996657	0.996655

computation of the FLI proceeds as follows. Let $\underline{\xi} = (y, z, p_y, p_z)$, let the vector field associated to (4.3) be denoted as

$$\dot{\underline{\xi}} = \underline{f}(\underline{\xi}), \quad \underline{\xi} \in \mathbf{R}^4,$$

and let the corresponding variational equations be

$$\dot{\underline{\eta}} = \left(\frac{\partial \underline{f}(\underline{\xi})}{\partial \underline{\xi}} \right) \underline{\eta}, \quad \underline{\eta} \in \mathbf{R}^4.$$

Having fixed an initial condition $\underline{\xi}(0) \in \mathbf{R}^4$, $\underline{\eta}(0) \in \mathbf{R}^4$, the FLI at a given time $T \geq 0$ is obtained by the expression

$$\text{FLI}(\underline{\xi}(0), \underline{\eta}(0), T) \equiv \sup_{0 < t \leq T} \log \|\underline{\eta}(t)\|,$$

where $\|\cdot\|$ denotes the Euclidean norm.

6.4. Applications. We proceed to implement the techniques described in Section 6.1, 6.2, 6.3 to the concrete samples provided by the Earth–Moon, Sun–barycenter, Sun–Vesta systems. The computations have been performed using **Mathematica**© as well as developing dedicated programs in a general-purpose programming language. The parameters associated to these three samples are listed in Table 2.

The values of the quantities introduced in Section 4, needed for the center manifold reduction, are listed in Table 3.

We analyze in detail the Sun–Vesta case, which presents several interesting features as the different parameters are varied. We start by computing the Poincaré surfaces of section of the center manifold associated to L_1 . We report in Figure 1 the Poincaré

TABLE 3. Quantities for the center manifold reduction associated to the Earth–Moon, Sun–barycenter, Sun–Vesta systems.

	Earth–Moon	Sun–barycenter	Sun–Vesta
γ_1	0.150948	0.01127	0.00334854
$\alpha(\gamma_1)$	-0.836898	-0.98873	-0.996651
a	-5.14772	-3.15056	-1.00363
b	5.14772	3.15056	1.00363
c	5.14772	3.15056	1.00363
λ_1	2.9321	2.13994	0.10407
ω_1	2.33441	1.85169	1.0036
ω_2	2.26886	1.77498	1.00181
s_1	14.9084	9.6584	0.79682
s_2	23.4324	12.6138	2.02523

sections in the plane (y, p_y) with only the gravitational effect, namely with $\beta = 0$ (no solar radiation pressure) and $A = 0$ (no oblateness). The maps show that the appearance of halo orbits occurs for an energy value approximately equal to $h = 0.35$ (more accurate computations will provide the bifurcation value $h = 0.3341$, compare with Table 4). For higher levels of the energy, the amplitude of the halo orbits increases as shown by the map at $h = 0.5$.

A different situation occurs when the radiation pressure and the oblateness are switched on, as shown in Figure 2 which reports the Poincaré sections for the case with $\beta = 10^{-2}$ and $A = 4.54776 \cdot 10^{-14}$. Indeed, we have noticed that the oblateness has a small effect, while the parameter β plays a major rôle in shaping the dynamics. In fact, a comparison between Figure 1 and Figure 2 shows that the sequence of bifurcations is completely different.

In Figure 2 we observe a regular behavior for $h = 0.04$, while already at $h = 0.05$ the dynamics experiences a first bifurcation with the appearance of halo orbits and simultaneous loss of stability of the planar Lyapunov orbit. A second bifurcation of unstable inclined orbits takes place at about $h = 0.1$; at this stage, the planar Lyapunov orbit regains stability (compare also with [8]), as shown in Figure 2 where the planar Lyapunov orbit is given by the outermost curve. For increasing values of the energy, the unstable families (which are located on the vertical axis of the plot for $h = 0.4$) collapse on the

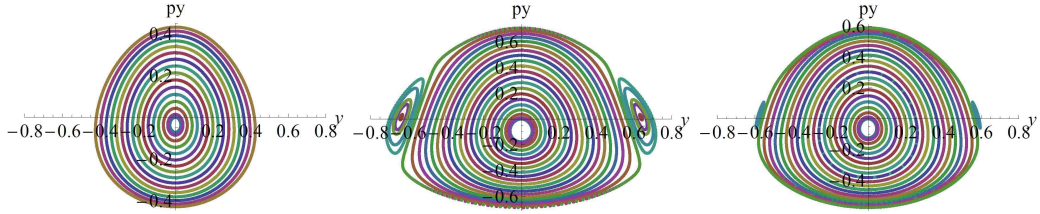


FIGURE 1. Poincaré sections of the center manifold associated to L_1 of the Sun–Vesta system on the plane (y, p_y) without solar radiation pressure (i.e., $\beta = 0$) and no oblateness (i.e., $A = 0$); different values of the energy are taken into account: $h = 0.2$ (left panel), 0.35 (middle), 0.5 (right).

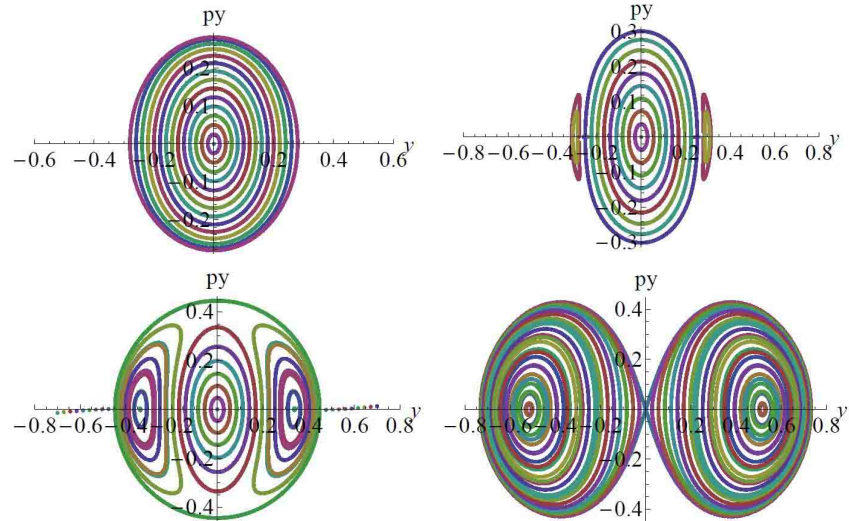


FIGURE 2. Poincaré sections of the center manifold associated to L_1 of the Sun–Vesta system on the plane (y, p_y) with $\beta = 10^{-2}$ and $A = 4.54776 \cdot 10^{-14}$; different values of the energy are taken into account: $h = 0.04$ (upper left panel), 0.05 (upper right), 0.1 (bottom left), 0.4 (bottom right).

vertical Lyapunov orbit at the center of the axes (see the bottom right panel of Figure 2). This corresponds to the third bifurcation, which is shown at about $h = 0.4$.

The above results are confirmed by the study of the model through frequency analysis, as shown in Figures 3 and 4.

In particular, in Figure 3 we provide the results of the frequency analysis for the Sun–Vesta case without solar radiation pressure and no oblateness in the (J_y^0, ω_r) plane with J_y^0 the initial condition and $\omega_r = |\omega_y/\omega_z|$. The first plot corresponds to $h = 0.2$ and it shows a regular behavior as it was found in the first plot of Figure 1. The occurrence of small halo orbits in the frequency analysis investigation corresponds to the two tiny

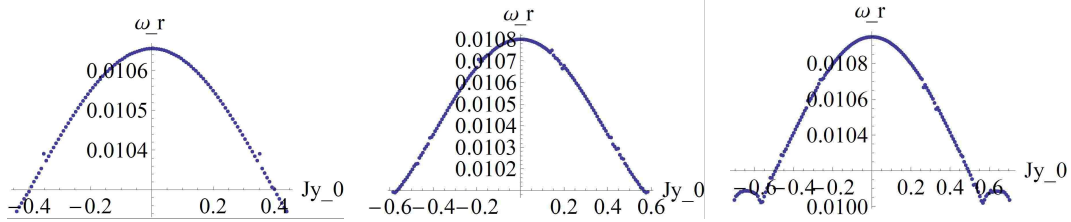


FIGURE 3. Frequency analysis in the plane (J_y^0, ω_r) for the Sun–Vesta case with $\beta = 0$, $A = 0$; different values of the energy are taken into account: $h = 0.2$ (left panel), 0.35 (middle), 0.5 (right).

bumps at the outermost sides of the plot for $h = 0.35$ in Figure 3; these bumps increase in size for $h = 0.5$, in full agreement with the corresponding plot of Figure 1.

The results of the investigation through frequency analysis in the case with solar radiation pressure and oblateness are provided in Figure 4, which corresponds to the Sun–Vesta case with $\beta = 10^{-2}$ and $A = 4.54776 \cdot 10^{-14}$. Again we find full agreement with the Poincaré maps provided in Figure 2. Precisely, the upper left panel of Figure 4 shows a regular behavior, while tiny bumps, corresponding to the bifurcation of the halo orbits for $h = 0.05$, are present in the upper right panel of Figure 4. The three island regimes occurring for $h = 0.1$ correspond to the central bump and the two left and right wings of the bottom left panel. Finally, for $h = 0.4$ we observe a singular behavior on the vertical axis of the bottom right panel of Figure 4, which corresponds to the vertical Lyapunov orbit at the origin of the coordinates in Figure 2.

The computation of the FLIs provides additional information: beside the overall structure of the phase space, it yields the regular or chaotic character of the different trajectories. In particular, we can locate the separatrices, which were not easily determined within the Poincaré maps (compare, e.g., Figure 2 bottom left and Figure 6 bottom left).

In Figure 5 we provide the results obtained computing the FLIs for the Sun–Vesta case without solar radiation pressure and no oblateness; the results must be compared with Figure 1 in order to distinguish the different orbits on the Poincaré maps and to determine their stability on the FLI plots. The color bar on the side of each plot gives the quantitative value of the FLI.

In Figure 6 we provide the results obtained computing the FLIs for the Sun–Vesta case with $\beta = 10^{-2}$ and $A = 4.54776 \cdot 10^{-14}$. Again, Figure 6 must be compared with Figure 2

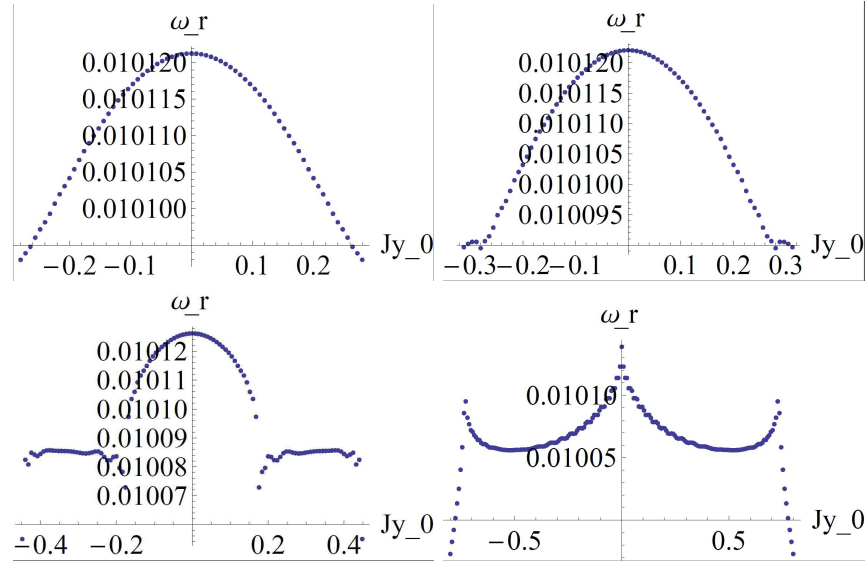


FIGURE 4. Frequency analysis in the plane (J_y^0, ω_y) for the Sun–Vesta case with $\beta = 10^{-2}$ and $A = 4.54776 \cdot 10^{-14}$; different values of the energy are taken into account: $h = 0.04$ (upper left panel), 0.05 (upper right), 0.1 (bottom left), 0.4 (bottom right).

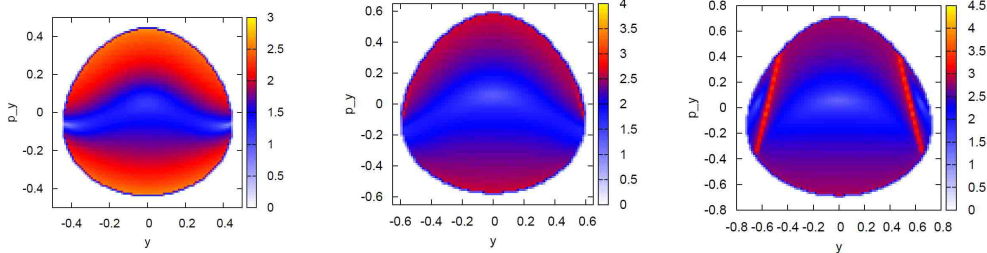


FIGURE 5. Fast Lyapunov Indicators for the Sun–Vesta case with $\beta = 0$, $A = 0$; different values of the energy are taken into account: $h = 0.2$ (left panel), 0.35 (middle), 0.5 (right).

in order to identify the various trajectories on the Poincaré sections and to characterize their stability on the FLI plots. It is remarkable how the FLI plots highlight also the separatrices as shown in particular in the bottom panels of Figure 6.

When the halo orbits are very tiny, a zoom becomes necessary, as shown in Figure 7, where we provide a magnification of the plots obtained in the cases with $\beta = 0$, $h = 0.35$ (left panel) and $\beta = 10^{-2}$, $h = 0.05$ (right panel).

In the panels of Figure 6 we notice some lighter regions which are mainly along the horizontal direction (compare with the bottom right panel); these zones do not have a

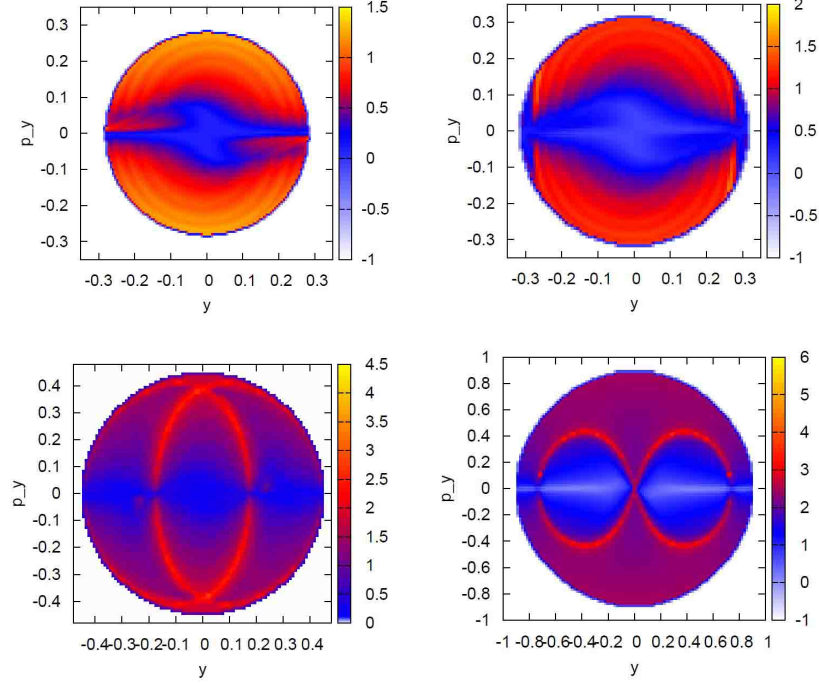


FIGURE 6. Fast Lyapunov Indicators for the Sun–Vesta case with $\beta = 10^{-2}$ and $A = 4.54776 \cdot 10^{-14}$; different values of the energy are taken into account: $h = 0.04$ (upper left panel), 0.05 (upper right), 0.1 (bottom left), 0.4 (bottom right).

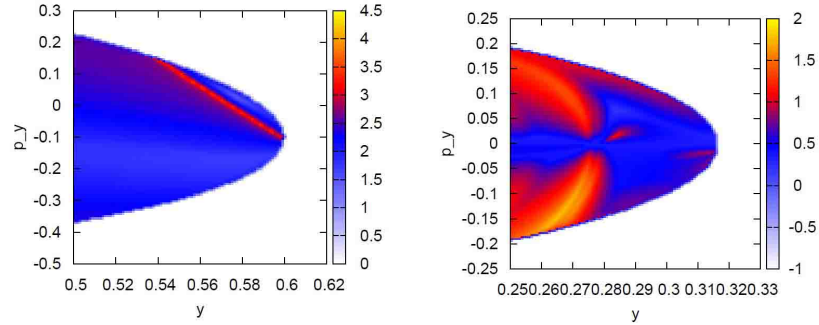


FIGURE 7. A zoom on the cases with $\beta = 0$, $h = 0.35$ (left panel) and $\beta = 10^{-2}$, $h = 0.05$ (right).

real dynamical meaning, but they are rather an artefact of the choice of the initial tangent vector, as the FLI strongly depends on this choice. In Figure 6 the tangent vector has been fixed as $(v_{px}, v_{py}, v_x, v_y) = (1, 0, 0, 0)$ and we observe that lighter regions occur in the direction perpendicular to the chosen tangent vector. A reliable description of the

TABLE 4. Numerical (num) and analytical (anal) value of the energy at which the bifurcation to halo orbits has taken place; the results are given for the Earth–Moon, Sun–barycenter, Sun–Vesta systems.

	L_1 num	L_1 anal	L_2 num	L_2 anal
Earth–Moon $\beta = 0, A = 0$	0.3026	0.3069	0.3776	0.3636
Earth–Moon $\beta = 0, A = 4.15559 \cdot 10^{-9}$	0.3026	0.3069	0.3776	0.3636
Sun–barycenter $\beta = 0, A = 0$	0.3333	0.3356	0.3377	0.3391
Sun–barycenter $\beta = 10^{-2}, A = 1.96782 \cdot 10^{-12}$	0.2793	0.2864	0.3759	0.3755
Sun–Vesta $\beta = 0, A = 0$	0.3341	0.3373	0.3346	0.3374
Sun–Vesta $\beta = 10^{-2}, A = 4.54776 \cdot 10^{-14}$	0.0422	0.0424	0.4451	0.4434

dynamical character of a specific region by means of the FLIs can only be obtained by comparing the plots produced using different tangent vectors in orthogonal directions or, alternatively, by increasing very much the accuracy of the computations. However, we remark that the analysis of Figure 6 suffices to distinguish the bifurcations as well as the main structures, like halo orbits or separatrices; further refinements go beyond the aims of the present work.

7. ANALYTICAL VERSUS NUMERICAL RESULTS

In this section we compare the results which are obtained implementing the analytical formulae (5.3)–(5.4) for the computation of the bifurcation thresholds with the numerical values obtained through the Poincaré maps or the FLIs.

The analytical and numerical bifurcation values for all three case studies (Earth–Moon, Sun–barycenter, Sun–Vesta) are listed in Table 4. The analytical results require the computation of the normal form as well as the computation of the thresholds at first order in the detuning as given by (5.3)–(5.4). The qualitative results are obtained looking at the bifurcations observed on the Poincaré sections as well as through the FLI maps (the results are also validated through the application of the frequency analysis).

From Table 4 we can draw the following conclusions.

- (i) The agreement between the analytical and numerical results is very satisfactory. The relative error between the theoretical and experimental values ranges between 10^{-2} and 10^{-3} .

- (ii) A first order estimate is already enough to get a good approximation of the bifurcation thresholds; this estimate requires a very little computational effort with respect to the qualitative analysis based on the Poincaré maps or the FLIs. Obviously, better results can be obtained computing higher order normal forms, but at the expense of dealing with more complex formulae.
- (iii) Switching on the solar radiation pressure provokes drastic changes for small mass parameters. In particular, in the Sun–Vesta case the first, second and third bifurcations take place at much lower values of the energy level, such that the other bifurcations become feasible. From the physical point of view, the reason for such a peculiar behavior is due to the balance between a smaller mass like that of an asteroid and the effect of the solar radiation pressure.
- (iv) The rôle of the oblateness is essentially negligible in all considered cases. This fact could have been inferred easily, but we believe worthwhile to derive a complete model, valid not only for the cases studied in the present paper, but also for general situations in which the small body could have a very irregular shape. Simple experiments show that in a Sun–asteroid sample, the oblateness becomes important only when the factor A is as large as $10^{-6} - 10^{-7}$. This parameter value does not apply to Vesta, but it might be of interest for other astronomical situations.

ACKNOWLEDGMENTS

We deeply thank Gerard Gomez for very useful suggestions and Danilo Stella for interesting discussions. M.C. and A.C. were partially supported by the European Grant MC-ITN Astronet-II, G.P. was partially supported by the European Grant MC-ITN Stardust. M.C., A.C., G.P. acknowledge GNFM/INdAM.

APPENDIX A. DERIVATION OF THE MEAN MOTION AROUND AN OBLATE PRIMARY

For completeness we derive here the formula for the mean motion of a massless body P under the gravitational effect of an oblate primary. Let us denote by M_P and A the mass and the oblateness coefficient of the primary, r represents the distance of P from the primary and \mathcal{H} is the angular momentum constant. Then, the effective potential (see, e.g., [1]) can be written as

$$V_{eff}(r) = \frac{\mathcal{H}^2}{2r^2} - \frac{M_P}{r} - \frac{M_P A}{2r^3},$$

whose derivative is

$$V'_{eff}(r) = -\frac{\mathcal{H}^2}{r^3} + \frac{M_P}{r^2} + \frac{3M_P A}{2r^4}.$$

The solutions of $V'_{eff}(r) = 0$ are given by

$$r = \frac{\mathcal{H}^2 \pm \sqrt{\mathcal{H}^4 - 6M_P^2 A}}{2M_P}. \quad (\text{A.1})$$

Taking into account that A is small, we can approximate the non-trivial solution of (A.1) by

$$r = \frac{\mathcal{H}^2}{M_P} \left(1 - \frac{3}{2} \frac{M_P^2 A}{\mathcal{H}^2}\right). \quad (\text{A.2})$$

Assume that the orbit of P is circular, say $r = a$, we have that $\mathcal{H}^2 = n^2 a^4$ which, together with (A.2) and the normalization of the units of measure such that $a = 1$, $M_P = 1$, provides:

$$n^2 = 1 + \frac{3}{2} A.$$

APPENDIX B. REDUCTION OF THE QUADRATIC PART

In this section we provide the details of the reduction of the quadratic part as performed in Section 3.2 in order to obtain the Hamiltonian (4.1) (equivalently (4.2)). The procedure is very similar to that explained in [11], to which we refer for a complete discussion; however, for self-consistency, we provide here some details containing the necessary amendments to encompass the oblate case with solar radiation pressure.

We start by computing the eigenvalues of M in (3.5); we denote by I_n the n -dimensional identity matrix. We notice that by defining $M_\lambda \equiv M - \lambda I_4$, we can write $M_\lambda = \begin{pmatrix} A_\lambda & I_2 \\ B & A_\lambda \end{pmatrix}$ with $A_\lambda = \begin{pmatrix} -\lambda & n \\ -n & -\lambda \end{pmatrix}$ and $B = \begin{pmatrix} -2a & 0 \\ 0 & -b \end{pmatrix}$. Then, the kernel of M_λ is given by the solution of $M_\lambda w = 0$ with $w = \begin{pmatrix} w_1 \\ w_2 \end{pmatrix}$ and $w_1, w_2 \in \mathbf{R}^2$. Simple computations show that the eigenvector of M is given by

$$(2n\lambda, \lambda^2 + 2a - n^2, n\lambda^2 - 2an + n^3, \lambda^3 + (2a + n^2)\lambda)^\top,$$

where λ is an eigenvalue of M (the superscript \top denotes the transposed).

Let us consider the eigenvectors associated to $\omega_1 = \sqrt{-\eta_1}$; from (3.6) we have $p(\lambda) = 0$, so that ω_1 satisfies the equation

$$\omega_1^4 - (2n^2 + 2a + b)\omega_1^2 + (n^4 - 2an^2 - bn^2 + 2ab) = 0.$$

Using $i\omega_1 = \lambda_1$, the eigenvector $u_{\omega_1} + iv_{\omega_1}$ associated to ω_1 is given by

$$\begin{aligned} u_{\omega_1} + iv_{\omega_1} &\equiv (2ni\omega_1, -\omega_1^2 + 2a - n^2, \\ &\quad -n\omega_1^2 - 2an + n^3, -i\omega_1^3 + (2a + n^2)i\omega_1)^\top, \end{aligned}$$

while for $\pm\lambda_1 = \sqrt{\eta_2}$ we obtain:

$$\begin{aligned} u_{+\lambda_1} &= (2n\lambda_1, \lambda_1^2 + 2a - n^2, \\ &\quad n\lambda_1^2 - 2an + n^3, \lambda_1^3 + (2a + n^2)\lambda_1)^\top \\ v_{-\lambda_1} &= (-2n\lambda_1, \lambda_1^2 + 2a - n^2, \\ &\quad n\lambda_1^2 - 2an + n^3, -\lambda_1^3 - (2a + n^2)\lambda_1)^\top. \end{aligned}$$

Let $C = (u_{+\lambda_1}, u_{\omega_1}, v_{-\lambda_1}, v_{\omega_1})$; we have

$$C^\top JC = \begin{pmatrix} 0 & D \\ -D & 0 \end{pmatrix}, \quad \text{where} \quad D = \begin{pmatrix} d_{\lambda_1} & 0 \\ 0 & d_{\omega_1} \end{pmatrix}$$

with d_{λ_1} and d_{ω_1} given by

$$\begin{aligned} d_{\lambda_1} &= -2\lambda_1((-4n^2 + 2a - b)\lambda_1^2 - 4n^4 + bn^2 + 6an^2 - 2ab + 4a^2), \\ d_{\omega_1} &= -\omega_1((-4n^2 + 2a - b)\omega_1^2 + 4n^4 - bn^2 - 6an^2 + 2ab - 4a^2). \end{aligned}$$

In order to obtain a symplectic change of variables, we re-scale by $s_1 = \sqrt{d_{\lambda_1}}$, $s_2 = \sqrt{d_{\omega_1}}$ and we require that $d_{\lambda_1} > 0$, $d_{\omega_1} > 0$. Finally, we re-scale (z, p_z) by $(\frac{1}{\sqrt{\omega_2}}, \sqrt{\omega_2})$. The final symplectic change of variables is given by the matrix whose columns are $u_{+\lambda_1}/s_1$, u_{ω_1}/s_2 , $v_{-\lambda_1}/s_1$, v_{ω_1}/s_2 .

APPENDIX C. CENTER MANIFOLD REDUCTION

Let H be a Hamiltonian function with 3 degrees of freedom, admitting an equilibrium point of type *saddle*×*center*×*center*. Let $\pm\lambda$, $\pm i\omega_1$, $\pm i\omega_2$ be the eigenvalues of the linearized system. Expanding the Hamiltonian around the equilibrium point in complex variables, we obtain a simpler Hamiltonian function of the form

$$H(q, p) = H_2(q, p) + \sum_{n \geq 3} H_n(q, p),$$

where

$$H_2(q, p) = \lambda q_1 p_1 + i\omega_1 q_2 p_2 + i\omega_2 q_3 p_3,$$

while $H_n(q, p)$ are homogeneous polynomials of degree n in the variables (q, p) . To decouple the hyperbolic direction from the elliptic one, we need to kill the monomials whose exponent in p_1 is different from that in q_1 . This procedure, which makes use of Lie series, allows one to get a first integral with level surface given by the center manifold. We

sketch below the procedure to find the canonical transformation, referring to [11] for full details.

Given a Hamiltonian H and a generating function G , we denote by \hat{H} the function³

$$\hat{H} \equiv H + \{H, G\} + \frac{1}{2!} \{\{H, G\}, G\} + \frac{1}{3!} \{\{\{H, G\}, G\}, G\} + \dots \quad (\text{C.1})$$

If G has degree 3, say $G = G_3$, comparing same orders in (C.1) provides

$$\begin{aligned} \hat{H}_2 &= H_2, \\ \hat{H}_3 &= H_3 + \{H_2, G_3\}, \\ \hat{H}_4 &= H_4 + \{H_2, G_4\} + \{H_3, G_3\} + \frac{1}{2!} \{\{H_2, G_3\}, G_3\}, \dots \end{aligned}$$

Next we look for G_3 such that \hat{H}_3 is in normal form. Expanding H_2, H_3, G_3 as

$$\begin{aligned} H_2(q, p) &= \sum_{j=1}^3 \eta_j q_j p_j, \\ H_3(q, p) &= \sum_{|k_q|+|k_p|=3} h_{k_q, k_p} q^{k_q} p^{k_p}, \\ G_3(q, p) &= \sum_{|k_q|+|k_p|=3} g_{k_q, k_p} q^{k_q} p^{k_p} \end{aligned}$$

for some coefficients $h_{k_q, k_p}, g_{k_q, k_p}, \eta_j$ and denoting by $\eta = (\lambda, i\omega_1, i\omega_2)$, we have

$$G_3(q, p) = \sum_{(k_q, k_p) \in \mathcal{S}_3} \frac{-h_{k_q, k_p}}{\langle k_p - k_q, \eta \rangle} q^{k_q} p^{k_p},$$

where \mathcal{S}_3 is the set of indexes (k_p, k_q) , such that $|k_p|+|k_q|=3$ and with the first component of k_p different from the first component of k_q . We proceed iteratively to higher orders up to a given order, say N , so that we obtain:

$$\hat{H}(q, p) = H^{(N)}(q_1 p_1, q_2, q_3, p_2, p_3) + R^{(N+1)}(q_1, q_2, q_3, p_1, p_2, p_3),$$

where $H^{(N)}$ is a polynomial of degree N and $R^{(N+1)}$ is a reminder of order $N+1$. Neglecting the reminder and setting $q_1 p_1 = 0$, we eliminate the hyperbolic component of $H^{(N)}$ and we obtain a 2 degrees of freedom Hamiltonian of the desired form. As remarked in [11], there are no small divisors in the above procedure, since $|\langle k_q - k_p, \nu \rangle| \geq |\lambda_1|$ for any $(k_p, k_q) \in \mathcal{S}_j$, $j \geq 3$.

³Curly brackets denote, as usual, the Poisson brackets ([7]).

TABLE 5. Coefficients up to degree 4 of the Hamiltonian restricted to the center manifold for the Sun–Vesta system with $\beta = 10^{-2}$. The exponents (k_1, k_2, k_3, k_4) refer to the variables (y, z, p_y, p_z) .

k_1	k_2	k_3	k_4	h_k
2	0	0	0	0.501797549378742
0	2	0	0	0.500906031584819
0	0	2	0	0.501797549378742
0	0	0	2	0.500906031584819
2	0	1	0	0.0014920550494420622
0	0	3	0	-0.000248666270046148
0	2	1	0	0.0003790464810461912
4	0	0	0	-0.02099512477285749
2	2	0	0	-0.010667382077111268
0	4	0	0	-0.001354993618855492
2	0	2	0	0.04199066782897781
0	2	2	0	0.010667253491139606
0	0	4	0	-0.003498979471471415
1	1	1	1	$2.81508155360122 \cdot 10^{-7}$
2	0	0	2	$1.8824017340799554 \cdot 10^{-7}$
0	2	0	2	$4.7821141283422436 \cdot 10^{-8}$
0	0	2	2	$-9.411646402154861 \cdot 10^{-8}$

Going back to real variables (y, z, p_y, p_z) , we obtain a Hamiltonian of the form

$$\tilde{H}(y, z, p_y, p_z) = \sum_{k_1, k_2, k_3, k_4 \in \mathbf{Z}} h_{k_1, k_2, k_3, k_4} y^{k_1} z^{k_2} p_y^{k_3} p_z^{k_4}.$$

The first few non–zero terms h_{k_1, k_2, k_3, k_4} of the Hamiltonian restricted to the center manifold are provided in Table 5.

REFERENCES

- [1] A. Celletti, *Stability and Chaos in Celestial Mechanics*, Springer-Verlag, Berlin; published in association with Praxis Publishing Ltd., Chichester, ISBN: 978-3-540-85145-5 (2010)
- [2] A. Celletti, C. Froeschlé, *On the determination of the stochasticity threshold of invariant curves*, Int. J. Bif. Chaos **5**, n. 6, 1713–1719 (1995)
- [3] A. Celletti, C. Froeschlé, E. Lega, *Frequency analysis of the stability of asteroids in the framework of the restricted, three-body problem*, Cel. Mech. Dyn. Astr. **90**, n. 3-4, 245–266 (2004)
- [4] A. Celletti, G. Pucacco, D. Stella, *Lissajous and Halo orbits in the restricted three-body problem*, Preprint (2014)
- [5] C.N. Douskos, V.V. Markellos, *Out-of-plane equilibrium points in the restricted three-body problem with oblateness (Research Note)*, Astronomy and Astrophysics **446**, 357–360 (2006)
- [6] C. Froeschlé, E. Lega, R. Gonczi, *Fast Lyapunov indicators. Application to asteroidal motion*, Cel. Mech. Dyn. Astr. **67**, 41–62 (1997)
- [7] H. Goldstein, *Classical Mechanics*, Addison-Wesley, 3rd edition (2001)

- [8] G. Gómez, J.M. Mondelo, *The dynamics around the collinear equilibrium points of the RTBP*, Physica D **157**, 283–321 (2001)
- [9] À. Jorba, A. Farrès, *Dynamics of a solar sail near Halo orbits*, Acta Astronautica **67**, n. 7-8, 979–990 (2010)
- [10] À. Jorba, A. Farrès, *On the high order approximation of the centre manifold for ODEs*, DCDS-B **14**, n. 3, 977–1000 (2010)
- [11] À. Jorba, J. Masdemont, *Dynamics in the center manifold of the collinear points of the restricted three body problem*, Physica D, **132**, 189–213 (1999)
- [12] J. Laskar, *Frequency analysis for multi-dimensional systems. Global dynamics and diffusion*, Physica D **67**, 257–281 (1993)
- [13] J. Laskar, C. Froeschlé, A. Celletti, *The measure of chaos by the numerical analysis of the fundamental frequencies. Application to the standard mapping*, Physica D **56**, 253–269 (1992)
- [14] C.D. Murray, S.F. Dermott, *Solar system dynamics*, Cambridge University Press (1999)
- [15] P. Oberti, A. Vienne, *An upgraded theory for Helene, Telesto, and Calypso*, Astronomy and Astrophysics **397**, 353–359 (2003)
- [16] A. Marchesiello, G. Pucacco, *Relevance of the 1:1 resonance in galactic dynamics*, Eur. Phys. J. Plus **126**, 104 (2011)
- [17] A. Marchesiello, G. Pucacco, *Equivariant singularity analysis of the 2:2 resonance*, Nonlinearity **27**, 43–66 (2014)
- [18] G. Pucacco, A. Marchesiello, *An energy-momentum map for the time-reversal symmetric 1:1 resonance with $\mathbb{Z}_2 \times \mathbb{Z}_2$ symmetry*, Physica D **271**, 10–18 (2014)
- [19] R.K. Sharma, P.V. Subba Rao, *Collinear equilibria and their characteristic exponents in the restricted three-body problem when the primaries are oblate spheroids*, Celestial Mechanics **12**, 189–201 (1975)
- [20] V. Szebehely, *Theory of Orbits*, Academic Press, New York and London (1967)

DEPARTMENTS OF MATHEMATICS, UNIVERSITY OF ROMA TOR VERGATA, VIA DELLA RICERCA SCIENTIFICA 1, 00133 ROMA (ITALY)
E-mail address: kayleigh.s@hotmail.it

DEPARTMENTS OF MATHEMATICS, UNIVERSITY OF ROMA TOR VERGATA, VIA DELLA RICERCA SCIENTIFICA 1, 00133 ROMA (ITALY)
E-mail address: ceccaron@mat.uniroma2.it

DEPARTMENTS OF MATHEMATICS, UNIVERSITY OF ROMA TOR VERGATA, VIA DELLA RICERCA SCIENTIFICA 1, 00133 ROMA (ITALY)
E-mail address: celletti@mat.uniroma2.it

DEPARTMENTS OF PHYSICS, UNIVERSITY OF ROMA TOR VERGATA, VIA DELLA RICERCA SCIENTIFICA 1, 00133 ROMA (ITALY)
E-mail address: pucacco@roma2.infn.it